Ionic excitation in low-energy charge-transfer collisions between He_2^+ and some diatomic molecules*

G. H. Bearman, J. D. Earl, R. J. Pieper, H. H. Harris, and J. J. Leventhal
University of Missouri-St. Louis, St. Louis, Missouri 63121
(Received 23 October 1975)

Absolute excitation cross sections for charge transfer in 11-eV (lab) collisions between He_2^+ ions and N_2, CO, O_2, and NO molecules have been determined by observing photons from the decay of excited ions formed in the collisions. The magnitudes of these cross sections are unusually large (greater than 10^{-16} cm^2) when the electron exchange process is resonant or nearly resonant. Vibrational state distributions of the product ions were also determined to be consistent with a vertical transition (Franck-Condon) model. Explanations for the large cross sections and observed state distributions are proposed.

I. INTRODUCTION

Charge transfer has been shown to be an effective pumping mechanism for producing laser action. The recent success of the charge-transfer nitrogen-ion laser,[1] which is pumped by the reaction

$$He_2^+ + N_2 \rightarrow N_2^+(B\,^2\Sigma_g^+) + 2He \qquad (1)$$

has prompted further study of this class of reactions. Since processes analogous to (1) may be considered as potential laser pumping mechanisms,[2] absolute excitation cross sections for production of specific vibronic states are desirable. Emission spectra from such processes, when observed under single collision conditions, can yield these cross sections. In this paper results of such measurements for reactions between He_2^+ ions and N_2, CO, O_2, and NO molecules are reported. A preliminary report[3] containing excitation cross sections for He_2^+-N_2 charge transfer at 5 eV has been published. These cross sections were based on normalization of Hα emission in He^+-H_2 collisions at 100 eV to previously reported results[4]; since that time optical calibration has been performed *in situ*, and this calibration indicates that the He_2^+-N_2 cross sections in Ref. 3 should be increased by about a factor of 3. Further details of absolute measurements are presented later in this paper.

When He_2^+ accepts an electron, the resulting He-He interaction is repulsive, so that the effective recombination energy (RE) of He_2^+ varies over a range of roughly 18.3–20.3 eV,[3] with maximum overlap with $He_2^+(X\,^2\Sigma_u^+(v=0))$ occurring at about 19 eV. It is expected then that charge-transfer processes such as reaction (1) would be resonant when the product ion state lies in the range 18.3–20.3 eV above the ground state of the neutral molecule; such is the case for $N_2^+(B\,^2\Sigma_u^+(v=0))$. Figure 1 shows energy-level locations of electronic states ($v=0$) for the diatomic molecular ions studied here[5]; the horizontal dashed lines are the limits of the He_2^+ RE. The vertical arrows indicate known band systems for each ion.[5a] From this figure it is clear that, on the basis of energetic considerations alone, emissions resulting from charge transfer in each of the four-collision systems may be expected, and these emissions are in fact observed with large cross sections. These large cross sections are attributed both to the three-body nature of the final state which results from the He-He repulsive interaction and to the energy resonance. Such a three-body final state has available more phase space than the two-body final state[6] of most charge-transfer processes.

Unlike most previous studies of vibrational distributions produced in charge-transfer colli-

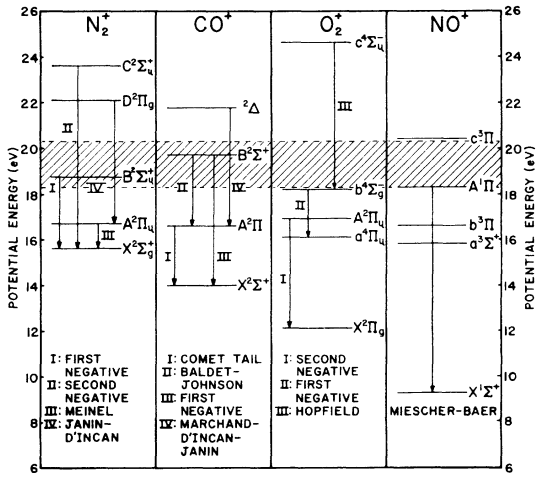

FIG. 1. Energy-level diagram for the indicated diatomic molecular ions. The locations shown are the lowest vibrational levels of each electronic state. Arrows indicate known band systems; these systems are identified at the bottom of the figure [Ref. 5(a)].

sions below ~ 10^8 cm/sec,[7] the He_2^+-N_2 system displays an $N_2^+(B)$ vibrational-state distribution consistent with Franck-Condon transitions from $N_2(X\,^1\Sigma_g^+(v=0))$ to $N_2^+(B)$. The non-Franck-Condon distribution in the earlier studies has been ascribed, with some success, to distortion of the target diatomic in the field of the incident ion,[7c] so that transitions occur from an extended neutral molecule. The Franck-Condon nature of the observed $N_2^+(B)$ vibrational distribution is then a consequence of the large cross section for the process, which permits electron transfer to the ion at large distance so that the target molecule is virtually undistorted when the transfer occurs. In such a circumstance the Franck-Condon factors calculated from the undistorted molecule are applicable. The cross sections for He_2^+-CO and He_2^+-O_2 are large enough so that the CO^+ and O_2^+ vibrational-state distributions are also consistent with the vertical transition model.

II. EXPERIMENTAL

A. Apparatus

The apparatus used in these experiments has been described in detail previously.[8] Ions are produced in a high-pressure electron-bombardment source and focused into a magnetic mass spectrometer by cylindrical electrostatic lenses. After mass selection the ion beam is directed into a collision cell containing neutral target molecules. Current is collected on a Faraday cup located immediately in back of the collision cell; typical values for 11 eV ions were 2×10^{-9} and 5×10^{-8} A for He_2^+ and He^+, respectively. Target gas pressures were maintained at 1 mTorr and monitored with a capacitance manometer.

Photons emerge from a 1.5× 20-mm slot in the collision cell and enter a Jarrell-Ash 0.25-m scanning monochromator whose entrance slit is located 1.25 cm from the beam trajectory. Both the entrance slit of the monochromator and the slot in the collision cell are oriented parallel to the beam. The detector was an EMI 9659 QAM photomultiplier cooled to 195 °K. Single-photon counting is employed and data are stored in a 256-channel analyzer. A stepping motor changes the wavelength setting of the monochromator in precise increments; dwell times of 10 sec per channel were usually employed. Filters were used when necessary to suppress second-order peaks in the spectrum, and the data were numerically corrected for the efficiency of the optical system and plotted using a Calcomp point plotter.

B. Calculation of cross sections

The cross section for production of any single line of a spectrum is given by

$$\sigma = (\mathcal{I}_s/\mathcal{I}_p)/nl, \tag{2}$$

where n is the target gas density, l is the scattering path length (2 cm in these experiments), $\mathcal{I}_p$ is the primary beam intensity in ions per second, and $\mathcal{I}_s$ is the (total) photon flux per second for the line. $\mathcal{I}_p$ was obtained from the Faraday-cup current and n from the capacitance manometer reading. Proper determination of $\mathcal{I}_s$ from the observed photon flux depends upon optical calibration and apparatus geometry, and it is this factor that is responsible for the major uncertainty in the determination of absolute cross sections. Preliminary results of this work presented in an earlier publication[3] were based on normalization of Hα intensities from 100-eV He^+-H_2 collisions to the cross section for this reaction reported by Isler and Nathan.[4] Their values were normalized to those reported by Gusev *et al.*[9] who in turn had based their cross sections on the earlier absolute measurements of Andreev *et al.*[10] Since Andreev's cross sections have been questioned,[11] it was decided to base the cross sections reported here on optical calibration and the geometry of the present apparatus.

Several simplifying assumptions were made: (i) Points along l, the path length, are the only sources and these sources emit photons isotropically. (ii) The effective, average solid angle subtended by a given monochromator entrance slit may be taken as the solid angle averaged over l. (iii) The resolution of the optical system is independent of wavelength. (iv) The species observed in these experiments have lifetimes which are short enough and laboratory speeds low enough to permit the assumption that none of the species observed escape the detection region.[8]

The optical system was calibrated using an Optronic Laboratories uv-40 deuterium lamp from 180 to 400 nm and a tungsten lamp from the same manufacturer from 300 to 900 nm. Appropriate filters were used during the calibration to eliminate scattered light. Agreement between efficiencies obtained using the two lamps was better than 5% in the overlapping wavelength region. The photon flux $\mathcal{I}_s$ was calculated from the formula

$$\mathcal{I}_s = [I_s(\lambda)/E(\lambda)]4\pi/\bar{\Omega}(s) \tag{3}$$

where $I_s(\lambda)$ is the observed photon count rate at the wavelength λ, $E(\lambda)$ is the optical system efficiency at that wavelength, and $\bar{\Omega}(s)$ is the average solid angle subtended by the slit. In this work all cross-section data were obtained using 1000-μm slits for which the solid angle is smaller than that of the monochromator.

Using the assumptions, calibration, and geometrical considerations described above, the cross

section for Hα and Hβ emission in 100 eV He^+-H_2 collisions was determined to be 1.9×10^{-17} and 2.1×10^{-18} cm^2, respectively. These values are approximately three times larger than those reported by Isler and Nathan[4] so that the cross sections in the preliminary version of this work should be increased by the same factor. It is believed that, while the relative values reported here should be considered accurate to within 20%, the absolute cross sections should be reliable to within a factor of 2.

It is difficult to use the above scheme to calculate cross sections for production of bands or sequences of bands which result from molecular transitions. The technique employed to obtain such cross sections was to use the value of the Hβ cross section above to determine a geometrical factor K in the relation

$$\sigma = K\frac{\sum I_s}{I_p}\frac{1}{n} \tag{4}$$

where I_p is the measured ion beam current and the summation in the numerator is taken over the wavelength settings which contribute to the Hβ peak; $\sum I_s$ is thus proportional to the area of the Hβ peak. Hβ was chosen rather than Hα because this emission is unpolarized while as much as 12% of the Hα emission can be polarized.[4] After K was determined as described above, the cross section for molecular emissions was calculated using the same slits and wavelength increment as in the Hβ experiments; $\sum I_s$ is then a measure of the band or sequence intensity, and σ is calculated from Eq. (4).

III. RESULTS

Figures 2–4 show spectra over the range 180–850 nm for He_2^+ collisions with N_2, CO, and O_2 at 11 eV (lab). For comparison, Figs. 2 and 4 also contain spectra from 11-eV He_2^+-N_2 and He^+-O_2 collisions, respectively. He^+-CO collisions at low energy produced no intense spectral features at these wavelengths. Figure 3 shows, in addition to the He_2^+-CO spectrum, the spontaneous emission spectrum from an unscattered CO^+ beam. This latter spectrum has no emissions which originate in the $B\,^2\Sigma^+$ state because the lifetime of this state is ~50 nsec[12] and most decays occur before the ions arrive at the (empty) collision cell. The comet tail bands, which originate in the $A\,^2\Pi$ state of CO^+ (lifetime ~2 μsec[12]), are present in this spectrum. Cross sections for production of some of the most prominent features of the spectra were calculated from the data and are indicated (in Å²) in Figs. 2–4.

The He_2^+-NO system was also examined in these studies and the spectrum observed was essentially featureless. Radiation in the wavelength range 180–850 nm from NO^+ has not been identified; however, the Miescher-Baer band system ($A \rightarrow X$) of NO^+ is known to produce emissions in the vacuum ultraviolet (1200–1700 Å).[5a,5b] Spectral scans at these wavelengths cannot be obtained with the

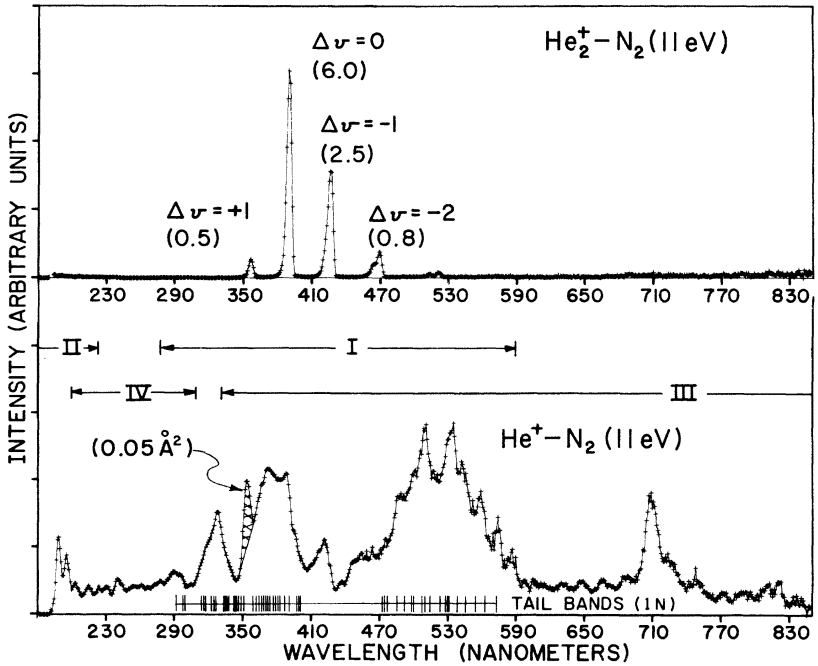

FIG. 2. Emission spectra from He_2^+-N_2 and He^+-N_2 collisions at 11 eV taken with 2-nm resolution. Known band systems of N_2^+ are indicated in the lower spectrum, and labeled as in Fig. 1. Emission cross sections in Å² for some prominent sequences are in parentheses.

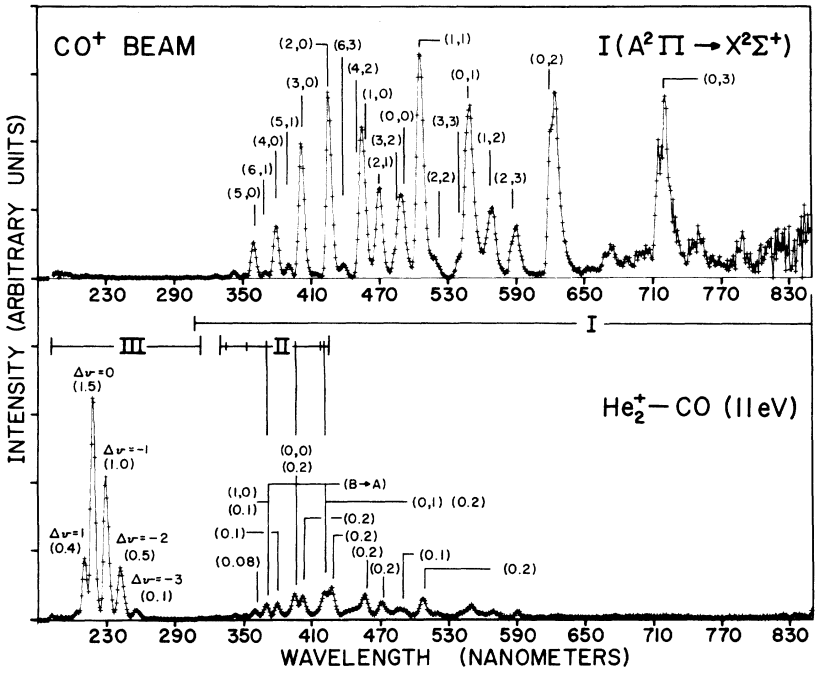

FIG. 3. Spontaneous emission spectrum from an unscattered CO^+ beam showing the comet-tail ($A \rightarrow X$) emissions of CO^+, and the emission spectrum from He_2^+-CO collisions at 11 eV, taken with 2-nm resolution. Known band systems of CO^+ are indicated in the lower spectrum, and labeled as in Fig. 1. Emission cross sections in $Å^2$ for some prominent bands are in parentheses.

present apparatus; however, by analogy with the other diatomic molecules studied here it is considered likely that the A state of NO^+ is produced in He_2^+-NO collisions. Use of a sodium salicylate coated window inside the vacuum chamber provides evidence for population of $NO^+(A)$ in He_2^+-NO collisions. Sodium salicylate fluoresces between 350 and 550 nm when irradiated by photons of wavelength less than 340 nm.[13] Observation of the fluorescent spectrum of sodium salicylate indicates that vuv photons are being produced by $NO^+(A \rightarrow X)$ transitions.

IV. DISCUSSION

A. N_2^+ emissions

The 11-eV He_2^+-N_2 spectrum shown in Fig. 2 is similar to that at 5 eV which was reported earlier. Comparison with the He^+-N_2 spectrum (Fig. 2) emphasizes the selective excitation of the N_2^+

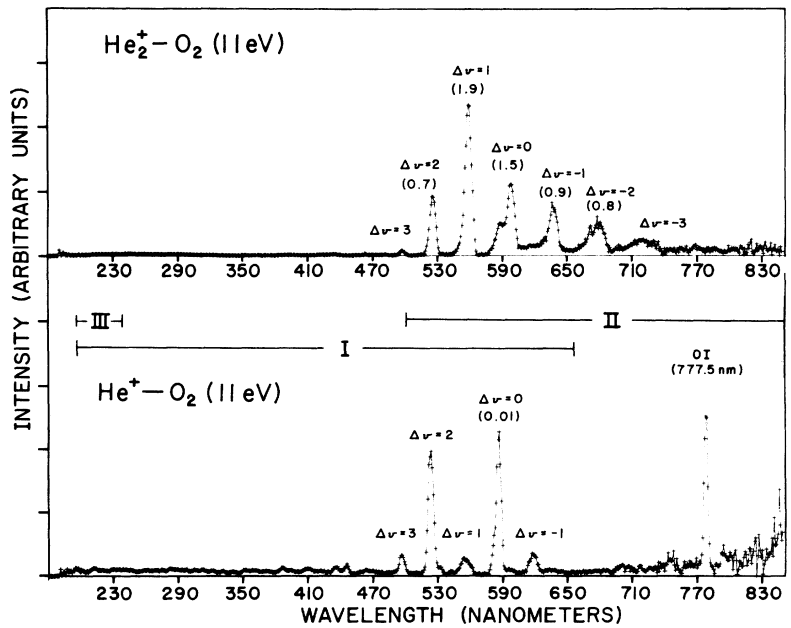

FIG. 4. Emission spectra from He_2^+-O_2 and He^+-O_2 collisions at 11 eV taken with 2-nm resolution. Known band systems of O_2^+ are indicated in the lower spectrum, and labeled as in Fig. 1. Emission cross sections in $Å^2$ for some prominent sequences are in parentheses.

product in He_2^+-N_2 collisions. The four known band systems of N_2^+ include transitions at wavelengths which are accessible in these experiments.[5a] In addition to the "tail bands"[3,7a] of $N_2^+(1N)$, a number of previously reported unresolved N_2^+ emissions occur in this region of the spectrum,[14] and the observation of Meinel emissions has been extended down to ~ 330 nm.[14b] The diffuse nature of the He^+-N_2 spectrum prevents unambiguous assignment of the transitions. It is clear, however, that the cross section for production of the indicated sequences of $N_2^+(1N)$ in the He_2^+-N_2 spectrum are much larger than the cross section for production of any single feature of the spectrum from He^+ impact. Note that the emission cross section for the cross-hatched peak in the He^+-N_2 spectrum [probably largely $\Delta v = +1$ of $N_2^+(1N)$] is only 0.05 Å^2. As discussed earlier the selective population of $N_2^+(B)$ has been attributed to a continuously variable recombination energy of He_2^+ in the range 18.3–20.3 eV. The recombination energy of He^+ on the other hand is 24.6 eV, sufficient to produce higher-lying states of N_2^+ which radiate at the wavelengths indicated in Fig. 2. Dissociative charge-transfer processes yielding ground-state atoms can also result from the high recombination energy of He^+.

On the basis of the He_2^+-N_2 spectrum in Fig. 2 it might be inferred that $N_2^+(A\,^2\Pi_u)$ is not produced in these collisions. It is certainly true that only insignificant emission from the Meinel system ($A \rightarrow X$) is observed; but, using the vertical transition model, it is calculated[15] that only about 8% of the Meinel emissions are detectable in the present apparatus. This is illustrated in Fig. 5 which shows the calculated relative intensities of the Meinel system out to 1160 nm. Several of the more intense (calculated) bands having wavelengths larger than 1160 nm are listed in the figure. The calculations include only effects of the overlap between $N_2^+(X\,^1\Sigma_g^+(v=0))$ and $N_2^+(A\,^2\Pi_u)$ and between $N_2^+(A\,^2\Pi_u)$ and $N_2^+(X\,^2\Sigma_g^+)$. Also shown in the figure is the spontaneous emission spectrum from an N_2^+ beam taken between 600 and 840 nm. This spectrum is consistent with the model calculation over the range covered. Although the photon flux from He_2^+-N_2 collisions is quite low at wavelengths larger than 600 nm, it is possible that $N_2^+(A)$ is produced but not observed here. Piper *et al.*[16] reached the conclusion that He_2^+-N_2 charge exchange produced $N_2^+(A)$ in their flowing afterglow apparatus. Nevertheless $N_2^+(B)$ is the preponderant radiating product observed.

Spectra taken at higher resolution than those

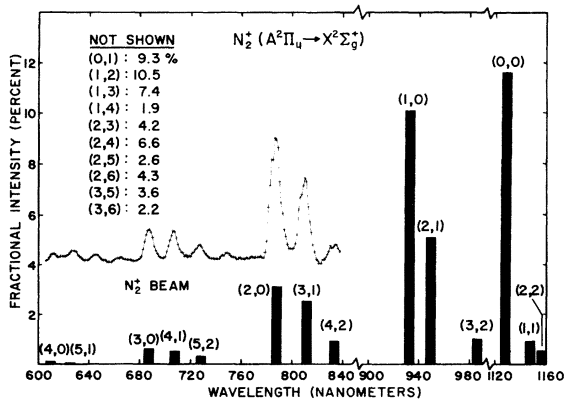

FIG. 5. Fractional intensities for the Meinel ($A \rightarrow X$) system of N_2^+ calculated under the assumption of vertical ionization $N_2(X) \rightarrow N_2^+(A)$, and vertical decay, $N_2^+(A) \rightarrow N_2^+(X)$. The Franck-Condon factors were obtained from Ref. 15. Also shown for comparison is a portion of the spectrum from an unscattered N_2^+ beam.

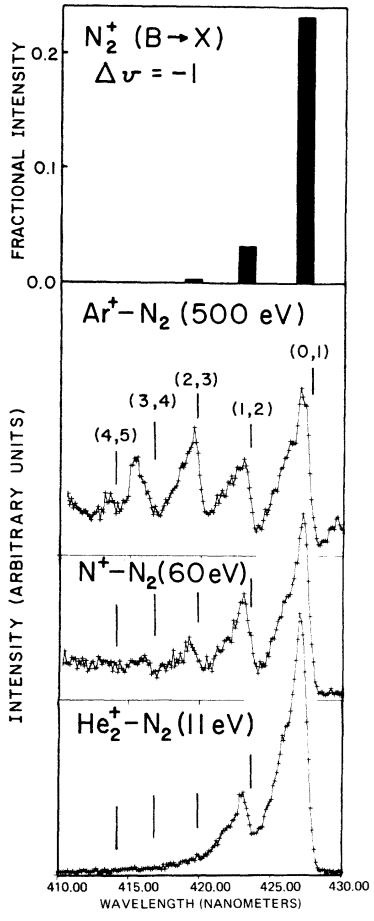

FIG. 6. Spectra of the $\Delta v = -1$ sequence of $N_2^+(1N)$ resulting from impact of Ar^+, N^+, and He_2^+ on N_2 taken at 0.4-nm resolution. Also shown are fractional intensities calculated under the assumption of vertical transitions. The fractional intensity scale was chosen so that the (0, 1) bar matched the (0, 1) band for He_2^+-N_2.

TABLE I. Excitation cross section for production of $N_2^+(B\,^2\Sigma_u^+(v'=i))$ in 11-eV He_2^+-N_2 collisions.

i	σ (Å^2)
0	8.9
1	1.0
2	...

shown in Fig. 2 may be used to obtain information on the vibrational state distribution in $N_2^+(B)$ that results from the collision process. Figure 6 shows the $\Delta v = -1$ sequence of the $N_2^+(1N)$ system produced by He_2^+ impact at 11 eV (lab) and by Ar^+ and N^+ impact. Also shown are the fractional band intensities calculated under the assumption of vertical ionization of $N_2(X\,^1\Sigma_g^+(v=0))$ followed by vertical $N_2^+(B \rightarrow X)$ transitions. The He_2^+ results closely match the model predictions while Ar^+ and N^+ produce vibrational distributions substantially different from the calculation. These differences are ascribed to the smaller cross sections for the Ar^+ and N^+ systems as discussed earlier.

The observed emission cross sections may be used in conjunction with the Franck-Condon factors[15] for decay to obtain excitation cross sections for production of specific vibrational levels of $N_2^+(B)$ in 11-eV He_2^+-N_2 collisions. Since the vibrational distribution in this case is consistent with vertical ionization, the Franck-Condon factors for ionization may be used to obtain these excitation cross sections using only the measured emission cross section for any sequence. The data for $\Delta v = 0$ were used; however, the $\Delta v = -1$ sequence independently yielded the same excitation cross sections. Of course, had it not been established that the ionizing transitions were vertical, it would have been necessary to resolve all of the sequences to obtain excitation cross sections for specific vibrational states. Table I is a listing of the excitation cross sections. The close correspondence between the total cross section (9.9 Å^2) calculated from the emissions in the $\Delta v = 0$ sequence alone and the total observed cross section (9.8 Å^2) may be taken as further evidence that the vertical transition model is applicable.

B. CO^+ emissions

Although the isoelectronic molecules CO and N_2 have similar chemical properties, the spectra produced by He_2^+ impact differ considerably. While the only significant N_2^+ emissions observed are from the $B \rightarrow X$ first negative system, the CO^+ spectrum includes emissions from the $B \rightarrow X$ (first negative), $B \rightarrow A$ (Baldet-Johnson), and $A \rightarrow X$ (comet-tail) systems. The Baldet-Johnson emissions occur in the same wavelength region as the comet-tail emissions but these two systems may be easily distinguished by comparison of the He_2^+-CO spectrum with the spontaneous emission from a CO^+ beam. The B state has a lifetime of ~50 nsec so that essentially all $CO^+(B)$ in the unscattered beam has decayed between the ion source and the collision cell (transit time ~10^{-5} sec). The A state on the other hand has a lifetime of ~ 2 μsec so that CO^+ emissions from the beam should be preponderantly in the comet-tail system (the A state being populated directly by electron impact and from $B \rightarrow A$ cascades). The He_2^+-CO spectrum should contain contributions from all nascent species in the collision cell. The features in the He_2^+-CO spectrum at 372 and 396 nm are not observed in the CO^+ beam, and, since these wavelengths coincide with the (1, 0) and (0, 0) bands of of the Baldet-Johnson systems,[5a,5c] it may be concluded that they are indeed due to $B \rightarrow A$ transitions. A higher resolution spectrum, shown in Fig. 7, suggests that the bands attributed above to the Baldet-Johnson system are violet degraded while the others are red degraded, in accordance with the known characteristics of these systems.[5a,5c] The electronic branching ratio from $CO^+(B)$ may be obtained from the total $B \rightarrow X$ and $B \rightarrow A$ intensities. These data indicate that 87% goes to $CO^+(X)$ and 13% goes to $CO^+(A)$ in reasonable agreement with recent determinations.[17]

Figure 7 also shows relative intensities of $B \rightarrow A$

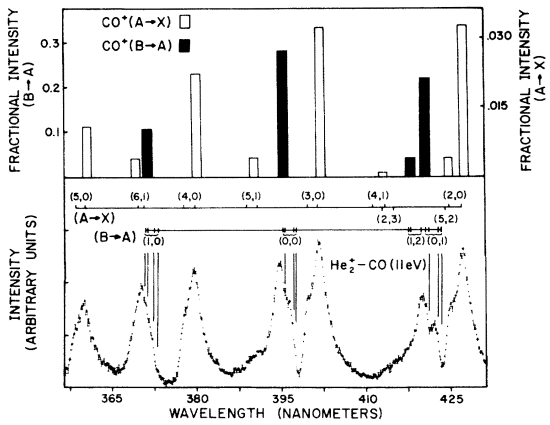

FIG. 7. Portion of spectrum from He_2^+-CO collisions at 11 eV taken with 0.4-nm resolution showing some of the $A \rightarrow X$ and $B \rightarrow A$ emissions. Also shown are the fractional intensities for the $A \rightarrow X$ and $B \rightarrow A$ systems of CO^+ calculated from the vertical transion model; Franck-Condon factors were obtained from Ref. 5(c). The ordinate scales for the fractional intensities were adjusted so that the relative heights of $A \rightarrow X(3, 0)$ and $B \rightarrow A(0, 0)$ matched the data.

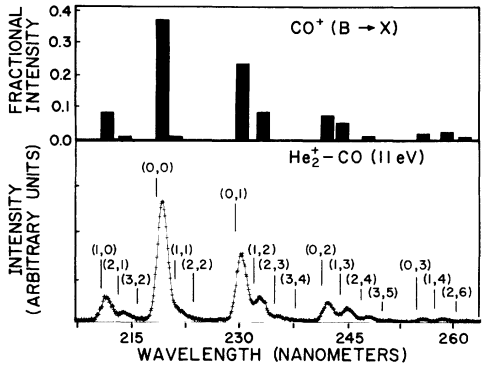

FIG. 8. Portion of the spectrum from He_2^+-CO collisions at 11 eV taken with 0.4-nm resolution showing $B \rightarrow X$ emission. Also shown are the fractional intensities calculated under the assumption of vertical transitions. The fractional intensity scale was chosen so that the (0, 0) bar matched the (0, 0) band.

and $A \rightarrow X$ bands calculated (as before) under the assumption of vertical ionization and vertical transitions in emission. The ordinate scales were adjusted so that the relative heights of the $A \rightarrow X$ (3, 0) band and the $B \rightarrow A$ (0, 0) band matched the data. The calculated fractional intensities indicate a considerably higher photon flux from $A \rightarrow X$ transitions than from $B \rightarrow A$ transitions (17:1), showing that $CO^+(A)$ is populated directly in the collisions as well as by cascading from the B state. The validity of the vertical transition model in He_2^+-CO charge-transfer collisions is further strengthened by comparing the higher resolution $CO^+(1N)$ spectrum with predicted intensities as shown in Fig. 8.

Table II is a listing of the cross sections for production of individual vibrational levels of the

TABLE II. Excitation cross sections for production of $CO^+(B\,^2\Sigma^+(v'=i))$ and $CO^+(A\,^2\Pi(v'=i))$ in 11-eV He_2^+-CO collisions.

	σ (Å^2)	
i	$CO^+(A\,^2\Pi)$	$CO^+(B\,^2\Sigma^+)$
0	0.6	3.0
1	1.3	1.3
2	1.6	0.2
3	1.5	0.03
4	1.0	···
5	0.6	···

A and B states of CO^+ in 11-eV He_2^+-CO collisions obtained in the same manner as those for production of $N_2^+(B)$. The cross sections for $CO^+(B)$ were obtained by adding the contributions from first negative and Baldet-Johnson emissions calculated from the (0, 0) band intensities of each of these systems; those for $CO^+(A)$ were based on the (5, 0) band of the comet-tail system in order to minimize contributions from cascading.[18] The sum of the cross sections listed in Table II for $CO^+(B)$ is slightly higher than the sum of the $B \rightarrow X$ and $B \rightarrow A$ emissions observed in these experiments. This discrepancy results from inclusion of unobserved emissions by the calculational technique. For example, Franck-Condon factors for the $B \rightarrow A$ system indicate that ~27% of the (0, v') intensity in this system should appear with $v'' \geq 2$; these bands, although they have not been observed, have been included in the above calculations. Similarly, the wide range of the comet-tail system and the large Franck-Condon factors for transitions beyond the present range of detection prevent a meaningful comparison of the cross

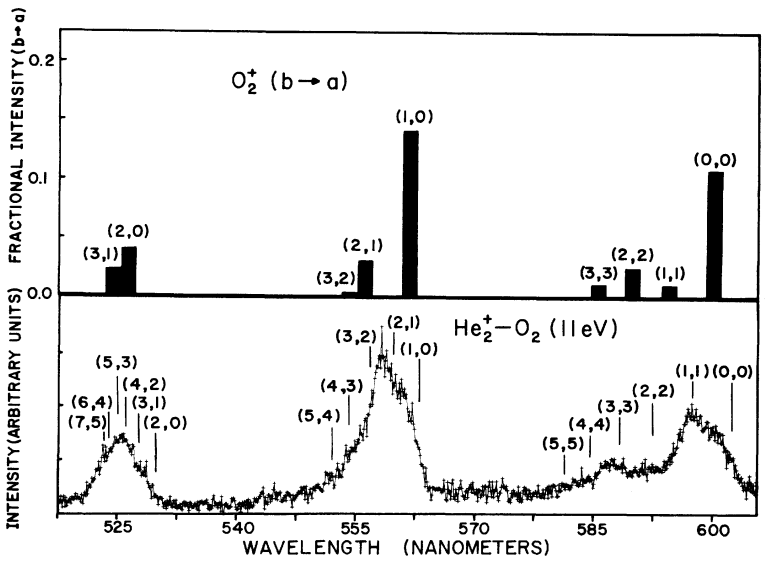

FIG. 9. Portion of the spectrum from He_2^+-O_2 collisions at 11 eV taken with 0.4 nm resolution showing some of the $b \rightarrow a$ emission. Also shown are the fractional intensities calculated under the assumption of vertical transitions; Franck-Condon factors were taken from Ref. 5(d). The fractional intensity scale was chosen so that the (1, 0) bar matched the height of the $\Delta v = +1$ sequence shown.

TABLE III. Excitation cross sections for production of $O_2^+(b\,^4\Sigma_g^-(v'=i))$ in 11-eV He_2^+-O_2 collisions.

i	σ (Å^2)
0	2.1
1	3.1
2	1.0
3	0.05

sections for production of $CO^+(A)$ in Table II with the observed emission cross sections.

Emission from He^+-CO collisions at 11 eV is weak in contrast to He^+-N_2 collisions which yield a rather high photon flux. CO^+ has four known band systems, the most recently discovered being the ($^2\Delta \rightarrow A\,^2\Pi$) system[19] shown in Fig. 1. No emissions could be assigned to this system for either He_2^+ or He^+ collisions with CO. N_2^+ has two band systems which originate in electronic states lying higher then the B state. In addition, unresolved emissions from N_2^+ at these wavelengths,[14] recently attributed to new (high-lying) electronic states,[20] have been observed. Analagous high-lying states of CO^+, if bound, evidently do not radiate within 180–850 nm.

C. O_2^+ emissions

As shown in Fig. 1 the $b\,^4\Sigma_g^-$ state of O_2^+ lies within the He_2^+ recombination energy "band". It is thus expected that significant yields of $O_2^+(b)$ could result from He_2^+-O_2 collisions and indeed strong $b \rightarrow a$ (first negative) emissions are observed. Figure 4 shows 11-eV He_2^+-O_2 and He^+-O_2 spectra. Emissions from He^+-O_2 collisions at higher kinetic energies have been reported previously[21]; Fig. 4 extends these results to 11 eV. The O I 777.5-nm line which dominates the higher-energy spectra has decreased in intensity and is now comparable to the $\Delta v = 0$ and +2 sequences of the $O_2^+(b \rightarrow a)$ system. This is consistent with the endoergic nature of the dissociative charge-transfer process which causes this emission. In addition to the rather strong first negative emissions from He_2^+-O_2 collisions, small yields of the $A \rightarrow X$ second negative system are also observed.

A higher resolution spectrum of the $\Delta v = 0$, +1 and +2 sequences of the first negative system of O_2^+ from 11 eV He_2^+-O_2 collisions is shown in Fig. 9. This resolution is not quite sufficient to separate individual bands as was possible for the N_2 and CO systems. Nevertheless, an estimate of the vibrational-state distribution may be made by comparison with the band intensities predicted from the vertical transition model. Since the cross section for production of O_2^+ emissions in He_2^+-O_2 collisions are comparable to those for N_2 and CO emissions, it is anticipated that the model also applies to O_2. Because individual bands were not resolvable in these data, the bars in Fig. 9 have been placed at the band origins.[5d] Comparison with the data suggests that vertical transitions also occur in this case, but this conclusion is weaker than for the N_2 and CO systems. Table III contains a listing of the excitation cross sections for 11-eV He_2^+-O_2 collision assuming vertical ionization and vertical decay; the calculations are based on the $\Delta v = 0$ sequence.

D. NO^+ emissions

As noted earlier, $NO^+(A \rightarrow X)$ emissions, though expected from He_2^+-NO collisions, cannot be observed directly in these experiments since they occur in the vacuum ultraviolet. An estimate of the cross section for production of these emissions can be obtained by measuring the fluorescence when a sodium salicylate coated window in the vacuum chamber is struck by photons from He_2^+-NO and from He_2^+-CO collisions. Only the first negative emissions of CO^+ can cause fluorescence of the phosphor[13] so that, assuming He_2^+-CO collisions yield no emissions at shorter wavelengths, the fluorescent yield of the coated window may be correlated directly to the total cross section for production of $CO^+(1N)$ emissions. If the quantum efficiency of the phosphor is the same for NO^+ ($A \rightarrow X$) and $CO^+(B \rightarrow X)$ emissions, the data show that the cross section for $NO^+(A \rightarrow X)$ emission is approximately 0.7 Å^2.

ACKNOWLEDGMENTS

The authors would like to thank Dr. B. J. Feldman, Dr. P. B. James, and Dr. G. R. North for many helpful discussions of this work.

*Research supported by the U. S. Energy Research and Development Administration under contract No. E(11-1)-2718.

[1](a) C. B. Collins and A. J. Cunningham, Appl. Phys. Lett. 27, 127 (1975); (b) C. B. Collins, A. J. Cunningham, and M. Stockton, Appl. Phys. Lett. 25, 344 (1974).

[2]R. A. Waller, C. B. Collins, and A. J. Cunningham, Appl. Phys. Lett. 27, 323 (1975).

[3]J. J. Leventhal, J. D. Earl, and H. H. Harris, Phys. Rev. Lett. 35, 719 (1975).

[4]R. C. Isler and R. D. Nathan, Phys. Rev. A 6, 1036 (1972).

[5](a) B. Rosen, *Spectroscopic Data Relative to Diatomic Molecules* (Pergamon, Oxford, 1970); (b) F. R. Gilmore, J. Quant. Spectrosc. Radiat. Transfer 5, 369 (1965); (c) P. H. Krupenie, Natl. Stand. Ref. Data Ser. (U.S.) 5 (1966); (d) P. H. Krupenie, J. Phys. Chem. Ref. Data 1, 423 (1972).

[6]L. M. Tannenwald, Proc. Phys. Soc. 87, 109 (1966).

[7](a) D. Brandt, Ch. Ottinger, and J. Simonis, Ber. Bunsengesenges. Phys. Chem. 77, 648 (1973); (b) G. N. Polyakova, V. F. Erko, A. V. Zats, Ya. M. Fogel', and G. D. Tolstolutskaya, Zh. Eksp. Teor. Fiz. Pis'ma Red. 11, 562 (1970) [JETP Lett. 11, 390 (1970)]; (c) M. Lipeles, J. Chem. Phys. 51, 1252 (1969); (d) J. H. Moore, Jr., and J. P. Doering, Phys. Rev. 177, 218 (1969).

[8]H. H. Harris and J. J. Leventhal, J. Chem. Phys. (to be published).

[9]V. A. Gusev, G. N. Polyakova, V. F. Erko, Ya. M. Fogel', and A. V. Zats, in *Abstracts of the Sixth International Conference on the Physics of Electronic and Atomic Collisions*, edited by I. Amdur (MIT Press, Cambridge, Mass., 1969), p. 809.

[10]E. P. Andreev, V. A. Ankudiov, and S. V. Bobashev, Opt. Spektrosk. 16, 187 (1964) [Opt. Spectroc. 16, 103 (1964)].

[11]E. W. Thomas, *Excitation in Heavy Particle Collisions* (Wiley, New York, 1972).

[12]R. A. Anderson, At. Data 3, 227 (1971).

[13]J. A. R. Samson, *Techniques of Vacuum Ultraviolet Spectroscopy* (Wiley, New York, 1967).

[14](a) R. F. Holland and W. B. Maier II, J. Chem. Phys. 55, 1299 (1971); (b) W. B. Maier II and R. F. Holland, J. Chem. Phys. 59, 4501 (1973).

[15](a) R. W. Nicholls, J. Res. Natl. Bur. Stand. (U.S.) 65A, 451 (1961); (b) T. F. Moran and L. Friedman, J. Chem. Phys. 42, 2391 (1965).

[16]L. G. Piper, L. Gundel, J. E. Velazco, and D. W. Setser, J. Chem. Phys. 62, 3883 (1975).

[17](a) W. C. Richardson and D. A. Setser, J. Chem. Phys. 58, 1809 (1973); (b) D. L. Judge and L. C. Lee, J. Chem. Phys. 57, 455 (1972); (c) G. M. Lawrence, J. Quant. Spectrosc. Radiat. Transfer 5, 359 (1965).

[18]See Franck-Condon factors in Ref. 5(c).

[19]J. Marchand, J. D'Incan, and J. Janin, Spectrochim. Acta 25A, 605 (1969).

[20](a) D. C. Cartwright and T. H. Dunning, Jr., J. Phys. B 8, L100 (1975); (b) E. W. Thulstrup and A. Anderson, J. Phys. B 8, 965 (1975).

[21]H. H. Harris, M. G. Crowley, and J. J. Leventhal, Chem. Phys. Lett. 29, 540 (1974).